The relationship of chain linearity of aromatic liquid-crystal polyesters to molecular orientation and stiffness of mouldings*

D. J. Blundell, R. A. Chivers†, A. D. Curson, J. C. Love and W. A. MacDonald

ICI Wilton Materials Research Centre, PO Box No. 90, Wilton, Middlesbrough, Cleveland TS6 8JE, UK

(Received 26 October 1987; revised 9 February 1988; accepted 11 February 1988)

Three aromatic liquid-crystal polyesters have been synthesized from monomer residues of x parts p-hydroxybenzoic acid and $\frac{1}{2}(1-x)$ parts each of isophthalic acid and hydroquinone, with $x=0.15$, 0.27 and 0.36. Chain linearity therefore increased with x. They were injection-moulded into tensile bars which had axial moduli that were found to increase with x. The bars were sectioned to reveal the oriented layer structure formed by the injection process. The molecular orientation within the layers was characterized by X-ray diffraction and then input into the Ward aggregate model to calculate predicted moduli for comparison with experimentally measured moduli. The analysis shows that, for higher x, the increase in modulus is mainly a consequence of the increase in molecular orientation within the layers.

(Keywords: liquid-crystal polymer; thermotropic; X-ray diffraction; aggregate model; tensile modulus; molecular orientation function)

INTRODUCTION

It is a characteristic of rigid-chain thermotropic liquid-crystal polymers that the molecular axes of the polymer chains closely follow the direction of the flowing mesophasic melt. Unlike conventional polymers, there is no strong entropic driving force for the chains to relax after the viscous flow field has been removed. Injection mouldings are thus very anisotropic and exhibit enhanced stiffness along the direction of predominant flow.

Sections cut through mouldings show that the flow patterns usually give rise to a layered morphology. Previous studies[1-3] of moulded thermotropic polymers have demonstrated that the most obvious division in the layer structure is between skin regions, which are highly oriented, and a core region, which has relatively poor overall orientation. The skin regions can often be subdivided into layers that can be visibly distinguished by dark/light banding. Scanning electron microscopy (SEM) and high-resolution optical microscopy indicate that there is a hierarchy of smaller oriented structures within each visually observed layer[1,2].

As a simplification of this layered structure, the injection mouldings can be considered to be microcomposites made up of layers in which the direction of reinforcement changes from layer to layer. The observed mechanical modulus of the overall moulding will reflect the integrated effect of the component layers. The important factors governing the modulus would be expected to be the thickness of the component layers and the direction and degree of orientation of the polymer chains within the layers. These factors will depend partly on the injection conditions and partly on the intrinsic response of the polymer chains to the flow conditions[4].

Most previous studies of these effects have been concerned with one polymer formulation and have considered the effects of the processing conditions. In this present study we wish to follow these same ideas but to focus on the variations that can be produced by changing the characteristics of the polymer at a molecular level. There are two main objectives:

(1) To explore how a change in the molecular linearity of a chain affects the degree of orientation and general layer structure in a moulding.

(2) To establish a quantitative relationship between orientation in the mouldings and the measured modulus.

In order to address the first objective, different aromatic polyesters have been synthesized from the following monomer residues:

Isophthalic acid (IA)

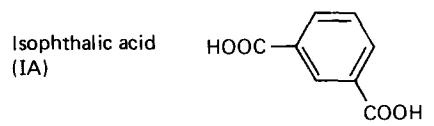

Hydroquinone (HQ)

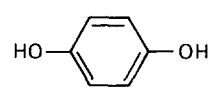

p-Hydroxybenzoic acid (HBA)

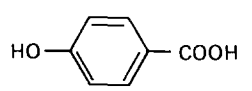

In this polymer series the molar fractions of the isophthalic acid (IA) and hydroquinone (HQ)

* Presented at Polymer Physics Group Conference 'Physical Aspects of Polymer Science', Reading, 9–11 September 1987

† To whom correspondence should be addressed

0032-3861/88/081459-09$03.00
© 1988 Butterworth & Co. (Publishers) Ltd.

components are kept equal and the remainder is made up of *p*-hydroxybenzoic acid (HBA). As the proportion of HBA is increased, *meta* links are introduced at the expense of *para* links and the chain becomes less linear. This family of polymers has also been studied by Erdemir *et al.*[5] from the point of view of the types of order and their fibre-forming characteristics. Our observations concur with their findings and show that, when the proportion of HBA is greater than about 20%, the melt state is a birefringent mesophase. For compositions of less than 20% HBA, a quiescent melt can revert to an isotropic state, although a subsequent shearing action can often re-establish the mesophase character. We have found that injection mouldings exhibit a systematic reduction in modulus as the proportion of HBA is reduced. For the present study we have selected three compositions (36, 27 and 15% HBA) for a detailed study. These three polymers allow us to explore mesophasic melts in which there is a significant change in the straightness of the chain. The 15% polymer is close to the borderline between liquid-crystal and conventional polymer behaviour. These polymers have been injection moulded under closely similar conditions into moulds in the form of tensile bar test specimens. Sliced sections have been cut in two directions through the thickness of the mouldings. The molecular orientation across the slices has been characterized by a combination of X-ray diffraction methods. Attempts have been made to characterize the orientation in terms of a Hermans orientation function using the spread of the intense equatorial diffraction arcs from the oriented chains. By this means we have been able to quantify both the direction and degree of orientation as a function of depth within the moulding. Finally, we have tried to link this molecular orientation information with the macroscopic modulus by using the formalism of the Ward 'aggregate model'[6]. We have assumed the simplified case of local uniaxial symmetry about the principal chain direction, which allows the compliance constants needed to describe the system to be reduced to five in number. In order to predict values for the modulus of the whole moulding, we used compliance values that Professor Ward has found applicable to the related rigid-chain copolyester of HBA and 2-hydroxy-6-naphthoic acid (HNA)[7].

The attempts to make a quantitative connection between molecular orientation and macroscopic modulus have necessitated using some assumptions in measuring the orientation and applying the aggregate model. Nevertheless, the level of agreement obtained gives some credence to the validity of the procedures and provides insight into how molecular orientation resulting from chain linearity contributes to reinforcement of a macroscopic moulding. In addition to the mechanical modelling, we also use the orientation data to clarify the nature of the dark/light banded appearance of the layers within the skin regions.

MATERIALS AND SPECIMENS

The polymers, of HBA/IA/HQ compositions 15/42.5/42.5, 27/36.5/36.5 and 36/32/32, were prepared in our laboratories. The polymers were injection moulded with feed temperatures between 330 and 350°C and nozzle temperatures between 340 and 360°C into a mould at 40°C. The mouldings were in the form of an ASTM type I tensile bar, nominally 3 mm thick and 13 mm wide in the central region. In this central, parallel-sided region, the skin naturally extended round the whole section. Therefore, before measuring the tensile moduli or looking at the structure, the width was trimmed down to about 10 mm to leave a section in which all layers are parallel to the *xz* plane of the specimen. Tensile moduli were determined at 0.25% axial strain on an Instron testing machine with a cross-head rate of 1 mm min^{-1}. The extensometer had a gauge length of 50 mm.

To provide samples for X-ray orientation studies, two 100 μm thick slices A and B were cut from a specimen as in *Figure 1* using a diamond Microslice saw. Another region of each specimen was cut along the centre line in the *yz* plane and polished in order to reveal the visual appearance of the layered structures by reflected light microscopy. This specimen was then ground down and polished on the reverse side to produce 8 μm thick sections similar to slice A. These were examined by transmitted light microscopy to examine the extinction characteristics in order to complement the X-ray orientation data.

CHARACTERIZATION OF ORIENTATION IN MOULDINGS

Definition of layer structure

There were two main stages in the characterization of orientation. In the first stage a microbeam X-ray camera and a diffractometer technique were used to define the location of the main layer structures and to give an overview of the nature of the orientation within each layer. The second stage used textural diffractometer measurements to quantify the direction and degree of orientation within each layer.

In the first step, a Norelco microbeam camera was used to take a series of X-ray photos across the thickness of each moulding by mounting the type-A slices perpendicular to the beam. The camera was fitted with a 100 μm diameter capillary collimator and photographs were taken at 100 μm intervals across the slice. This allowed changes in orientation to be detected with a spatial resolution of about 100 μm. In order to assist in defining the location of the layer regime, the camera survey was supplemented by making the following type of topographical scan with a diffractometer.

A Philips Vertical Diffractometer was used with 1/30°

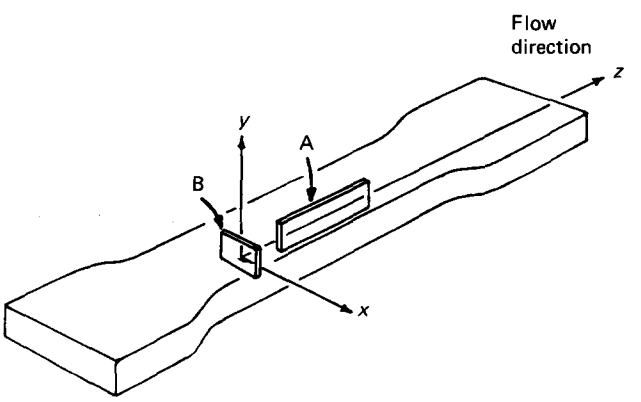

Figure 1 Diagram showing location of slices cut from tensile bar specimens

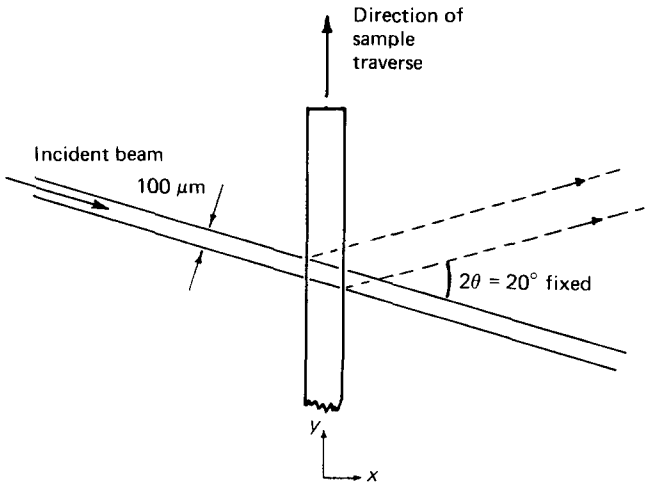

Figure 2 Diagram showing arrangement for the transverse topographical scan of slice A

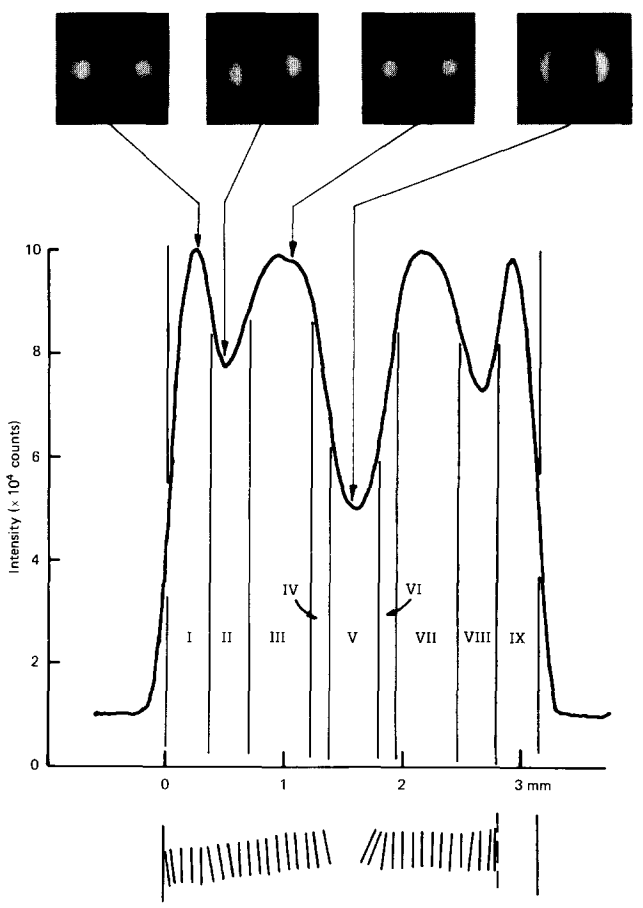

Figure 3 Topographical scan across the 36% HBA sample. Selected microbeam X-ray photographs are superimposed on the scan. Below is shown the principal optical axis deduced with a polarizing microscope

divergence slit. This produced a slit beam about 100 μm wide at the sample position. The A-type slices were mounted along the goniometer axis in a holder fitted with an actuator motor that allowed the sample to be accurately positioned in the beam. The diffractometer angle was set at $2\theta = 20°$, which is close to the peak intensity associated with scatter seen in the X-ray photographs. The intensity was recorded while the sample was translationally stepped across the beam as in *Figure 2*.

Examples of the X-ray photographs and the topographical scans are shown in *Figures 3–5*. In the most oriented case in *Figure 3*, the X-ray photographs are typical of an oriented fibre and confirm that the chain orientation is along the injection direction of the moulding. The arrangement of the sample in the topographical scans is such that the detector monitored the intensity of the equator of the photographs at the position where the intense equatorial spots occur. The variations in the intensity in the topographical profile correspond to changes in orientation in the moulding. A reduction in intensity corresponds to a decrease in the degree of orientation relative to the principal chain axis or a movement in the direction of principal chain axis away from the axis of the moulding.

The 36% HBA results shown in *Figure 3* gave the most dramatic changes in the topographical intensity. Moving in from the edge, the photographs clearly show that the dip between the first two peaks corresponds to a layer where there is a drop in the degree of orientation. The deep intensity dip in the middle of the moulding is associated with very confusing X-ray patterns, with sudden changes in direction of orientation, where in some cases the mean molecular axis is predominantly transverse to the injection direction. Consideration of all the photographs, the topographical scans and the optical appearance led to the conclusion that this moulding can be conveniently represented by the nine layers marked I to IX in *Figure 3*, which are arranged symmetrically about the centre line.

The features in the topographical scan of the 27% HBA sample shown in *Figure 4* are much less marked and the

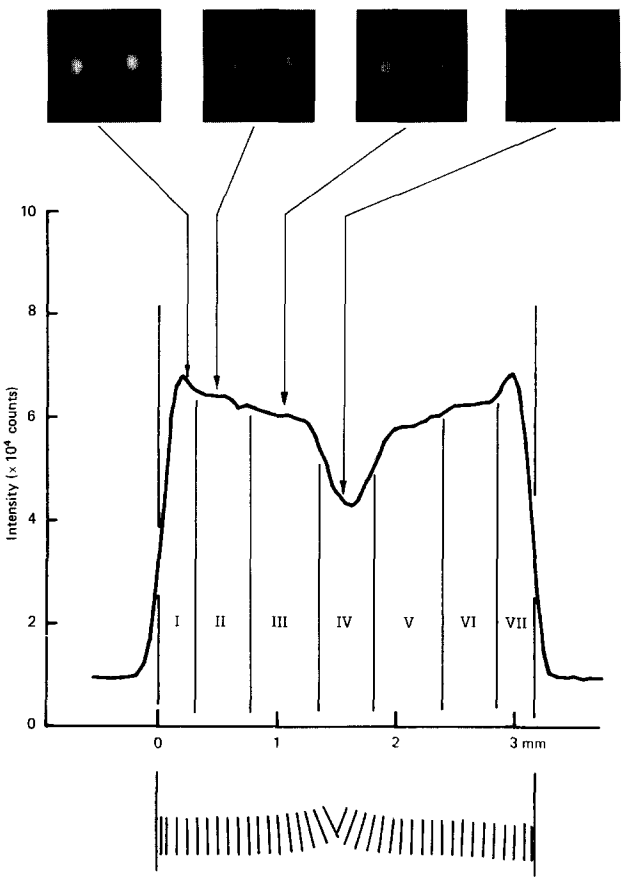

Figure 4 Topographical scan across the 27% HBA sample. Selected microbeam X-ray photographs are superimposed on the scan. Below is shown the principal optical axis deduced with a polarizing microscope

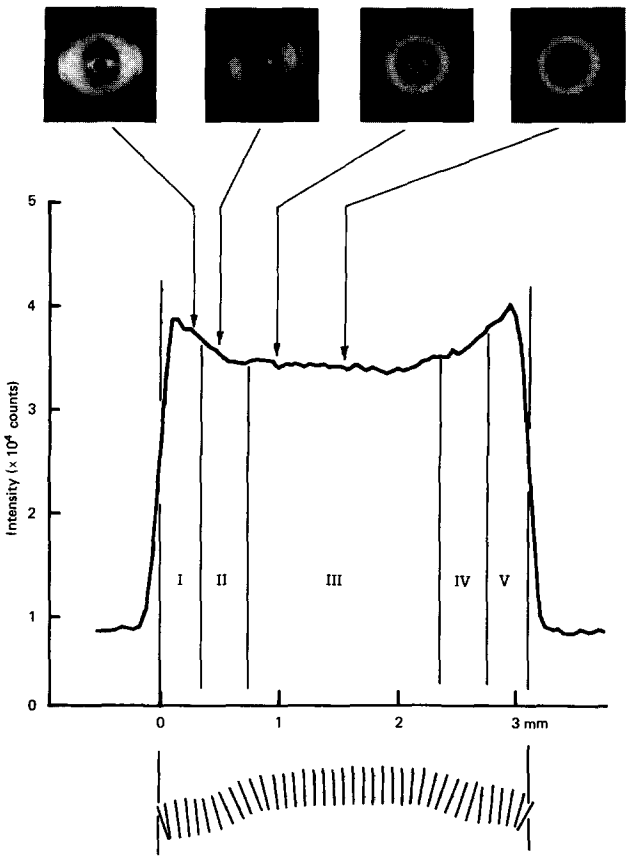

Figure 5 Topographical scan across the 15% HBA sample. Selected microbeam X-ray photographs are superimposed on the scan. Below is shown the principal optical axis deduced with a polarizing microscope

overall level of orientation poorer. The outer peaks correspond to the regions of highest orientation. The orientation falls gradually from the edge to the centre and the dip in intensity is again associated with confused orientation. The results suggest that this sample can be represented by the seven layers marked I to VII.

The topographical scan of the 15% HBA sample in *Figure 5* is almost featureless. The level of orientation in the photographs is closer to that expected in mouldings of a conventional polymer with only the surface layers showing clear orientation. It was decided that this moulding could be represented by the five layers marked I to V.

Quantification of orientation

In order to apply the mechanical model described below, it is necessary to know the spread of the angle ϕ_c between the chain axes and the principal direction of orientation as defined in *Figure 6*. The methods for doing this using X-ray diffraction are well established for crystalline polymers[8]. For samples with axial symmetry, the most convenient approach is to measure intensity variation of a strong equatorial (*hk*0) reflection. For the case of a simple orthorhombic polymer crystal, the intensity profile $I(\phi_a)$ would then allow the following relevant averages to be computed:

$$\overline{\cos^2\phi_a} = \frac{\int_0^{\pi} I(\phi_a)\cos^2\phi_a \sin\phi_a \, d\phi_a}{\int_0^{\pi} I(\phi_a)\sin\phi_a \, d\phi_a} \quad (1)$$

$$\overline{\cos^4\phi_a} = \frac{\int_0^{\pi} I(\phi_a)\cos^4\phi_a \sin\phi_a \, d\phi_a}{\int_0^{\pi} I(\phi_a)\sin\phi_a \, d\phi_a} \quad (2)$$

where ϕ_a is the angle between the principal chain direction and the normal to a (1 0 0) crystal plane. We can express the averages of ϕ_b with the (0 1 0) plane similarly.

For an orthorhombic crystal cell, the averages relative to the *a*, *b* and *c* crystal axes are related by:

$$\overline{\cos^2\phi_a} + \overline{\cos^2\phi_b} + \overline{\cos^2\phi_c} = 1 \quad (3)$$

This relationship leads to the derived equations (A.1)–(A.5) in Appendix 1. These equations allow the statistical spread of the chain axes (ϕ_c) to be calculated from the experimentally determined averages relating to the *a* and *b* axes as in equations (1) and (2) above.

In the case of non-crystalline polymers, the spread in the axis of the equatorial diffraction can no longer be rigorously related to the spread in the chain direction in the manner used for crystalline order. However, apparently meaningful results have been obtained by making the assumption that the direction of the interchain diffraction giving rise to the intense equatorial arcs closely corresponds to a normal to the chain axes[9,10]. Mitchell and Windle[11,12] have critically examined this assumption and have concluded that the correspondence is reasonable when the overall orientation is poor, but tends to underestimate the chain orientation when the orientation becomes high. The assumption becomes poor when the intrinsic spread of the diffraction due to the chain structure becomes comparable with the spread due to disorientation. In the present work we have chosen to adopt this assumption and have applied the above relationships for crystalline orientation directly to the more diffuse diffraction effects given by the three polymers. In making this assumption, the ϕ_a and ϕ_b in the above orientation averages are identical, since the *a* and *b* axes become equivalent to the direction perpendicular to the mean chain axis.

The three present polymers do in fact exhibit a range of crystalline order. *Figure 7* shows diffractometer 2θ traces along the equatorial direction taken from near the edges of the type-A slices. The 36% HBA sample gives diffuse, amorphous scatter with a maximum at $2\theta = 20°$. The 27% HBA and 15% HBA samples give an increasing amount of sharp crystalline diffraction superimposed on an

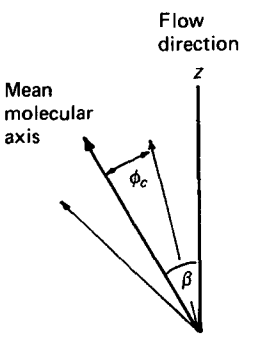

Figure 6 Diagram showing the spread of the molecular axes relative to the sample axis

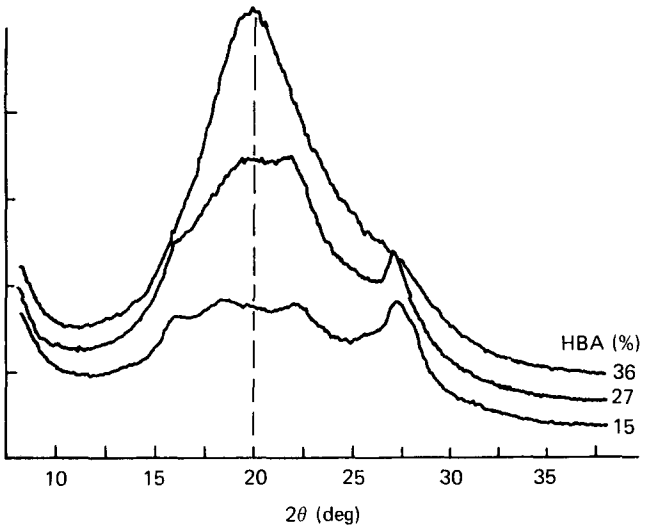

Figure 7 Equatorial X-ray diffractometer scans taken from the skin regions of the type-A specimens

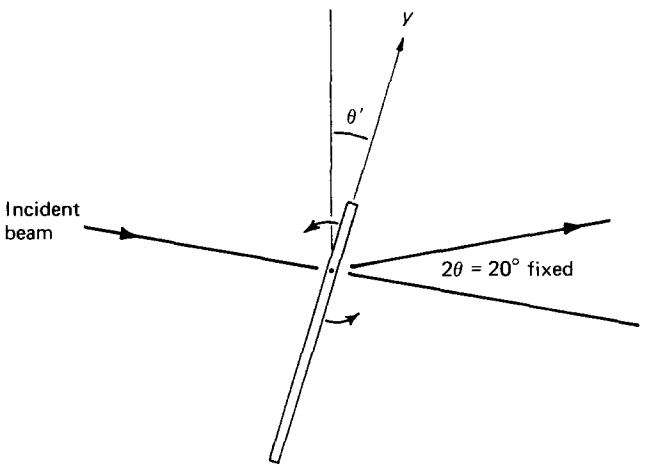

Figure 8 Diagram showing the arrangement of type-B specimens for the textural scans on the X-ray goniometer

amorphous halo. It has been shown[5] that the crystalline contribution is associated with residue sequences of the type $[IA–HQ]_n$. However, even in the 15% HBA sample, the crystalline diffracting species are still in a minority compared with the non-crystalline material. For consistency it was therefore decided to make the textural analysis at $2\theta=20°$. In all three polymers this angle corresponds to the peak of the equatorial diffraction emanating from the non-crystalline regions.

The textural measurement required for the orientation analyses effectively involves scanning round the equatorial arc in the X-ray fibre patterns. Experimentally this was achieved by mounting the type-B slice in a diffractometer as in *Figure 8* with the x (sideways) direction along the goniometer axis. The sample was positioned vertically so that the beam intercepted at the desired depth position y on the sample. The intensity was then recorded at $2\theta=20°$ while the sample was rotated about the goniometer axis (i.e. scanned with θ' movement of diffractometer). The background level for this scan was derived by stopping the θ' scan at selected points and obtaining a 2θ scan, similar in profile to those shown in *Figure 7*. On each of these 2θ scans, a straight line was constructed between the intensities at $2\theta=12°$ and 38°. The position of this baseline at $2\theta=20°$ was taken as the background intensity at the appropriate position on the textural θ' scan. After subtraction of the background, the resulting intensity profile was corrected for absorption effects by taking appropriate account of the thickness of sample traversed by the incident and reflected beams.

This measurement was repeated at positions, y, that corresponded to the middle of the selected layer structures indicated in *Figures 3–5*. In order to improve the signal-to-noise ratio, it was necessary to compromise the resolution of the textural scan by using a 1/6° divergent slit. This resulted in a beam 0.5 mm wide at the sample. Since this is slightly larger than some of the layers in the sample, it will tend to smooth out slightly some of the fluctuation in degree of orientation from layer to layer within the sample.

An example of a corrected intensity profile taken from near the edge of the 15% HBA sample is shown in *Figure 9* plotted against angle of rotation θ'. The position $\theta'=0$ in this figure corresponds to the point where the zy plane of the type-B slice bisected the angle between the incident and diffracted rays.

Two aspects of the orientation were deduced from this information. First, the deviation angle β was noted between the point of maximum intensity and the $\theta'=0°$ position. For a sample where the principal direction of chain alignment was along the axis of the moulding, one would expect β to be zero. Hence β is a measurement of deviation of the mean chain axis from the axis of the moulding.

Having decided on β, the intensity profile was used to calculate the orientation averages $\overline{\cos^2\phi_a}$ and $\overline{\cos^4\phi_a}$ using equations (1) and (2), where the position $\phi_a=90°$ was taken as the point of maximum intensity. These orientation averages for the vectors normal to the chain axes were substituted in equations (A.1)–(A.5) in Appendix 1 to calculate the various orientation averages relating to the chain axes themselves. Some slight fluctuations were found between data taken from symmetrically equivalent positions on opposite sides of the centre line of the type-B slices. In order to simplify the

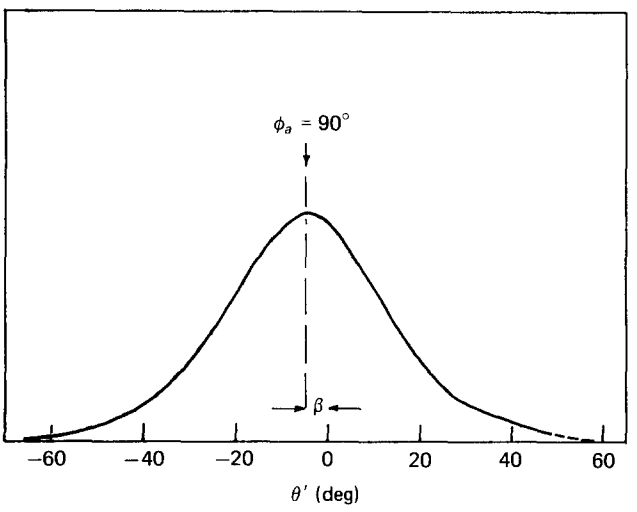

Figure 9 An example of an X-ray textural scan for the 15% HBA sample after correcting for background and absorption

Table 1 Orientation data for 36% HBA sample

Layers	I, IX	II, VIII	III, VII	IV, VI	V
Thickness (mm)	0.35	0.32	0.51	0.14	0.42
f_c	0.82	0.79	0.82	0.79	0.52
$\overline{\sin^4\phi_c}$	0.07	0.08	0.07	0.08	0.22
$\overline{\cos^4\phi_c}$	0.83	0.80	0.83	0.80	0.58
$\overline{\sin^2\phi_c \cos^2\phi_c}$	0.05	0.06	0.05	0.06	0.10
β (deg)	3	8	3	3	(0)
$1/s_{33}$ (GN m^{-2})	10.8	9.3	10.8	9.3	4.7

Table 2 Orientation data for 27% HBA sample

Layers	I, VII	II, VI	III, V	IV
Thickness (mm)	0.31	0.46	0.57	0.40
f_c	0.71	0.70	0.68	0.37
$\overline{\sin^4\phi_c}$	0.12	0.13	0.14	0.31
$\overline{\cos^4\phi_c}$	0.74	0.73	0.71	0.47
$\overline{\sin^2\phi_c \cos^2\phi_c}$	0.07	0.07	0.08	0.11
β (deg)	3.5	4	7	(0)
$1/s_{33}$ (GN m^{-2})	7.3	7.1	6.4	3.7

Table 3 Orientation data for 15% HBA sample

Layers	I, V	II, IV	III
Thickness (mm)	0.37	0.37	1.56
f_c	0.45	0.26	0.001
$\overline{\sin^4\phi_c}$	0.26	0.38	0.53
$\overline{\cos^4\phi_c}$	0.53	0.39	0.20
$\overline{\sin^2\phi_c \cos^2\phi_c}$	0.11	0.12	0.13
β (deg)	10	18	(0)
$1/s_{33}$ (GN m^{-2})	4.1	3.2	2.5

results, data from symmetrically related positions of the slices were averaged.

The averaged results associated with each of the identified layers are shown in *Tables 1–3*. The tables also list the Hermans orientation factor $f_c = \frac{1}{2}(3\cos^2\phi_c - 1)$. The results reaffirmed the trends shown in the X-ray photographs. There is the very marked fall-off in overall orientation between samples as the linearity of the polymer chain is reduced. There are also the systematic changes between the surface and centre of each sample. Of special interest is the correlation in the 36% HBA sample between the orientation parameters and the profile of the topographical scan in *Figure 2*. The dip in intensity associated with layers II and VIII is seen to be associated with a slight fall in degree of orientation and also an increased deviation in the chain direction away from the moulding axis, represented by an increase in β.

It should be pointed out that there is an implied assumption above that there is axial symmetry of the chain orientations about the mean molecular axis. However, the actual determination of f_c is based on a measurement that views the chains from the side along the x axis and no account is taken of the perpendicular view along the y axis. In fact X-ray photographs taken from a fragment from the skin region indicate that the degree of orientation as seen from the y direction is slightly poorer. However, this difference appears small compared with the differences found by varying the HBA content of the polymer and has therefore been ignored for the purpose of the following calculations of stiffness. Similarly there are small variations in the layer structure along a moulding; these have also been ignored.

OPTICAL EXAMINATION OF STRUCTURE

Reflected light micrographs obtained from the polished section taken along the yz plane of the centre line of the mouldings are shown in *Figure 10*. The fine scratchmarks are an artefact of the polishing process ripping fibrillar strands from the oriented structure. The grosser underlying dark/light banding bears a loose relationship to the topographical X-ray scans shown in *Figures 3–5*.

The correlation is clearer in the more complex banding in the 36% HBA case, where there is a lighter band associated with layers II (and VIII), which is bordered by darker bands associated with layers of higher orientation and higher intensity in the X-ray scan. This visual banded appearance does not depend on the viewing angle and is therefore primarily the result of a scattering effect rather than a difference in reflectivity.

When observed between crossed polarizers it is possible to find extinction directions that define the principal optical axes. These directions are marked underneath the topographical scans shown in *Figures 3–5*. These observations do not provide information on the strength of the birefringence, but only on the apparent principal axes as seen from the two-dimensional section. For instance, in the core region the principal molecular axis may in fact be predominantly perpendicular to the section. However in the surface regions where the banding is visible in the 36% HBA sample it will be noted that the vector marked on *Figure 3* correlates well with the variation in β found from X-rays.

The enhanced light scattering associated with the lighter band appears to be linked with a lower degree of molecular orientation. Previous microscopic studies[1–3] of layered structures of thermotropic polymer mouldings have shown that there is a hierarchy of substructures of decreasing size within the layers that tend to echo the shape and orientation of the melt flow. It is presumed that the light scattering effect giving rise to the banded appearance is associated with the domain substructures whose size is comparable with the wavelength of light.

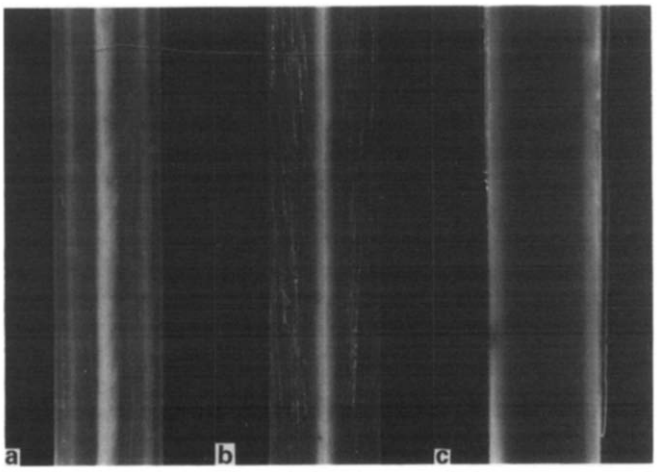

Figure 10 Reflected light micrographs of polished sections: (a) 36% HBA; (b) 27% HBA; (c) 15% HBA

The above correlation suggests that the scatter is due to a fluctuation in molecular orientation between such domains which causes a spatial fluctuation in polarizability. The very high birefringence of these molecules will cause any deviation in molecular orientation to produce a significant change in the resolved polarizability perpendicular to the mean molecular axis. The light banded layers thus probably represent regions where the fluctuation in transverse polarizability between domains is more pronounced.

MECHANICAL MODELLING

The aggregate model, derived by Ward[6], treats a macroscopic polymer specimen as an aggregate of highly oriented units, the orientations of which may vary. The mechanical properties of the specimen can then be derived by averaging the properties of the unit over the orientation distribution of units within the specimen. The averaging may be performed in either of two ways depending on the particular situation. Either a uniform stress is assumed throughout the specimen and compliances are summed (the 'Reuss average') or a uniform strain is assumed and stiffnesses are summed (the 'Voigt average'). Amongst studies on several polymers, Ward and coworkers have looked extensively at biaxially drawn poly(ethylene terephthalate) sheet for which orientation averaging was performed by Raman spectroscopy and refractive index measurement[13]. Using the properties of the most highly one-way drawn sheet as those of the unit, their nine experimental compliances for orthotropic sheets with different draw ratios lay mostly within the ranges defined by the Reuss and Voigt averages.

In the present work we adopt two simplifying assumptions in our use of the aggregate model. First, the polymers are assumed to show uniaxial (transversely isotropic) behaviour; and, secondly, we have performed the averaging in two stages, initially over individual layers within a specimen and then combining the layers. In each stage we used a different average as described below.

Previous work on thermotropic liquid-crystalline polymers has shown their tendency to behave in a fibrous manner. Indeed, they are frequently observed to behave similarly to fibre-reinforced composites, for example in the orientation behaviour resulting from moulding, and hence the term 'self-reinforcing polymer' has been applied. It is thus reasonable to assume fibre symmetry within the units and also in the layers, which all possess the same fundamental orientation and are aggregates of these units. Brody and Ward[14], considering fibre-reinforced composites compression moulded so as to give a uniform orientation, obtained good agreement between calculation and experiment using this assumption for both fibres and the composite article.

Three levels of structure are considered here. At the smallest scale is the unit, which is a collection of highly oriented molecules sufficient to give equatorial X-ray diffraction. The next scale up is the layer, which is assumed uniform across the entire width of the specimen and within which the units have an angular spread about an average orientation. Reasonable uniformity within the layers is confirmed by the optical studies, and the orientations themselves have been determined by X-ray diffraction. At the largest scale, the entire specimen is considered as a laminate of layers, symmetrically disposed about the centre.

We have used the aggregate model to derive the properties of the layers from the units. The assumption was made of uniform stress throughout each layer and hence a Reuss average was used. This is in agreement with the findings of Brody and Ward[14] on short-fibre-reinforced systems, and is also the lower bound to the calculated value of modulus. On combining the layers, however, uniform strain is assumed—the layers cannot move independently of each other—as is described by 'laminate theory'[15].

The following mechanical properties were assumed for the basic unit, regardless of composition[7]:

Axial modulus, E_3	100 GN m^{-2}
Transverse modulus, E_1	2 GN m^{-2}
Poisson's ratios, ν_{21}, ν_{13}	0.4
Shear modulus, G	1 GN m^{-2}

Compliances, s, were derived from these and applied in the equations of the aggregate model (Reuss average) to calculate the compliances of a layer, s'. These equations are standard and are given in Appendix 2.

The matrix of s' was inverted to give c', the stiffness of the layers. The reason for this is that, under uniform stress, compliances must be used, whereas under uniform strain, it is stiffness that must be considered.

The layers could not be combined exactly as calculated, though, because it was observed that the mean molecular orientation direction was not along the specimen axis at all times. The angle between this mean orientation direction and the axis was called β. The axes of the layers with respect to which the properties have been calculated above are based on the mean orientation direction as the z' axis. In order to find the stiffness along the specimen axis, therefore, the component of stiffness at angle β to the reference axis must be found:

$$c''_{33} = (\sin^4\beta)c'_{11} + (\cos^4\beta)c'_{33} + 2\cos^2\beta\sin^2\beta(c'_{13} + 2c'_{44}) \quad (4)$$

where a single prime refers to the layer axes and double primes to the specimen axes.

Finally the layers of thickness t_i were combined under the assumption of uniform strain to give the specimen axial modulus:

$$E = \frac{\sum_{i=1}^{n} (c''_{33})_i t_i}{\sum_{i=1}^{n} t_i} \quad (5)$$

Results of calculations for E for the three specimens are given in *Table 4* together with the experimental values.

Table 4 Comparison of experimental and predicted moduli

Composition (% HBA)	Experimental modulus (GN m^{-2})	Predicted modulus (GN m^{-2})
15	3.7	3.5
27	7.8	6.9
36	14.9	10.0

Very good agreement can be seen between experimental and calculated results, especially considering the approximations made in the calculations and the basic unit properties. Since the properties of a unit had been taken as approximate round numbers, further calculations were performed to observe the effect of changing these, using the orientations and layers measured for the 36% HBA system. Poisson's ratios were not varied since they are constrained to lie in a restricted range, but the other three parameters were systematically changed, one at a time while holding the others constant. Smooth variation of specimen modulus was observed with changes in the axial, lateral and shear moduli of the units. The relative magnitudes of varying each of these can be seen by considering the effect on the specimen modulus of a 10% increase in the individual unit modulus from the value used in the main calculations. Whereas a 10% increase in the lateral (E_1) and shear (G) moduli each give rise to an increase of about 5%, a 10% increase in the axial modulus of the unit leads to a rise of less than 1% in the specimen modulus. The implication of this, as has been observed before[14], is that, in a system with imperfect overall alignment, the precise value of a much-higher modulus (lower compliance) along the fibrous units is insignificant in determining the modulus of a macroscopic specimen of material.

There is an experimental reason why the predicted stiffness of the 36% HBA system is lower than that measured. This is that the orientation function of the units is being underestimated in this most highly oriented system in which the distribution of angles is small. There are two causes of this underestimation. Probably the more important is the finite size of the equatorial maximum even when the system diffracting is perfectly oriented[12]. What we observe is the convolution of this finite maximum with the function representing the range of angular orientation. This decreases the magnitude of the true orientation function by an indeterminate amount. The other cause is also broadening of the equatorial maximum, this time by convolution of the finite beam width with the true orientation function. The effect of a relatively broad beam will also make the apparent orientation function smaller than in reality.

The calculations were all performed with β in the central, core, layer set at 0°. It was by no means certain from the diffraction results that this was the case, and it was also suspected that significant orientation may exist out of the plane of the slice used for the diffraction experiments. Consequently, the calculations were repeated for a variety of β values from 0 to 90° in the core layer of each specimen for all three materials. A steady and almost insignificant variation in modulus was found. In the 36% HBA material, the modulus dropped by about 4% as β increased from 0 to 90°. In the 15% HBA material, the change was negligible.

CONCLUSIONS

There is very reasonable agreement between the experimentally observed axial moduli of the mouldings and the predicted values obtained by applying the aggregate model to the experimentally observed orientation data. This gives confidence in the validity of the approach and in the several assumptions that have been made at the various stages of the deduction process.

Of particular interest is the fact that the mechanical parameters assumed for the basic unit in the aggregate model were originally assigned for the fully linear HBA–HNA copolymers. The success in predicting properties for the present less linear systems indicates that the precise details of the molecule do not in themselves significantly influence the stiffness of a moulding. The most important factor is the degree of orientation attained.

There is a clear overall trend for the less linear molecules to produce less orientation and hence lower axial moduli. There is, however, a difference in the nature of the orientation between the 15% HBA case and the other two more linear polymers. In the 15% HBA moulding there is a more gradual reduction from the surface to the core and the core has no significant net orientation in the injection direction. In the other two samples, there is a clear distinction between the highly oriented skin regions and the less well oriented core. In these cases the increase in chain linearity produces a significant increase in orientation in the layer structures. There is, however, very little change in the relative thicknesses of the skin and core regions between these two samples. Thus the observed modulus increase with increased chain linearity is essentially a consequence of higher orientation. The orientation data also demonstrate that the banded appearance of the layers in the skin regions is associated with a small change of degree of orientation between layers.

ACKNOWLEDGEMENT

The experimental assistance of D. R. Tamblin was much appreciated.

APPENDIX 1

Axial orientation averages

The axial orientation averages can be expressed as follows:

$$\overline{\cos^2\phi_c} = 1 - 2\overline{\cos^2\phi_a} \quad \text{(A.1)}$$

$$\overline{\sin^2\phi_c} = 1 - \overline{\cos^2\phi_c} \quad \text{(A.2)}$$

$$\overline{\sin^4\phi_c} = 1 - 2\overline{\cos^2\phi_c} + \overline{\cos^4\phi_c} \quad \text{(A.3)}$$

$$\overline{\cos^2\phi_c \sin^2\phi_c} = \overline{\cos^2\phi_c} - \overline{\cos^4\phi_c} \quad \text{(A.4)}$$

$$\overline{\cos^4\phi_c} = 1 - 4\overline{\cos^2\phi_a} + 2\overline{\cos^4\phi_a} + \overline{\cos^2\phi_a \sin^2\phi_a} \quad \text{(A.5)}$$

APPENDIX 2

Derivation of compliances in units and layers from the aggregate model[6]

In what follows, the convention has been adopted that no prime refers to a unit and a single prime refers to a layer.

Unit compliances:

$$s_{33} = 1/E_3$$

$$s_{11} = 1/E_1$$

$$s_{13} = -\nu_{13} s_{33}$$

$$s_{12} = -\nu_{21} s_{11}$$

$$s_{44} = 1/G$$

Layer compliances:

$$s'_{33} = I_1 s_{11} + I_2 s_{33} + I_3(2s_{13} + s_{44})$$

$$s'_{11} = \tfrac{1}{8}(3I_2 + 2I_5 + 3)s_{11} + \tfrac{1}{4}(3I_3 + I_4)s_{13} + \tfrac{3}{8}I_1 s_{33} + \tfrac{1}{8}(3I_3 + I_4)s_{44}$$

$$s'_{13} = \tfrac{1}{2}I_3 s_{11} + \tfrac{1}{2}I_4 s_{12} + \tfrac{1}{2}(I_1 + I_2 + I_5)s_{13} + \tfrac{1}{2}I_3 s_{33} - \tfrac{1}{2}I_3 s_{44}$$

$$s'_{12} = \tfrac{1}{8}(I_2 - 2I_5 + 1)s_{11} + I_5 s_{12} + \tfrac{1}{4}(I_3 + 3I_4)s_{13} + \tfrac{1}{8}I_1 s_{33} + \tfrac{1}{8}(I_3 - I_4)s_{44}$$

$$s'_{44} = (2I_3 + I_4)s_{11} - I_4 s_{12} - 4I_3 s_{13} + 2I_3 s_{33} + \tfrac{1}{2}(I_1 + I_2 - 2I_3 + I_5)s_{44}$$

where I_1 to I_5 are given by:

$$I_1 = \overline{\sin^4\phi_c}$$

$$I_2 = \overline{\cos^4\phi_c}$$

$$I_3 = \overline{\cos^2\phi_c \sin^2\phi_c}$$

$$I_4 = \overline{\sin^2\phi_c}$$

$$I_5 = \overline{\cos^2\phi_c}$$

REFERENCES

1 Sawyer, L. C. and Jaffe, M. *J. Mater. Sci.* 1986, **21**, 1897
2 Weng, T., Hiltner, A. and Baer, E. *J. Mater. Sci.* 1986, **21**, 744
3 Thapar, H. and Bevis, M. *J. Mater. Sci. Lett.* 1983, **2**, 733
4 Ide, Y. and Ophir, Z. *Polym. Eng. Sci.* 1983, **23**, 261
5 Erdemir, A. B., Johnson, D. J. and Tomka, J. G. *Polymer* 1986, **27**, 441
6 Ward, I. M. *Proc. Phys. Soc.* 1962, **80**, 1176
7 Ward, I. M., private communication
8 Alexander, L. E., 'X-ray Diffraction Methods in Polymer Science', Wiley, New York, 1969
9 Biangardi, H. J. *J. Polym. Sci., Polym. Phys. Edn.* 1980, **18**, 903
10 Von Falkai, B., Spilgies, G. and Biangardi, H. J. *Angew. Makromol. Chem.* 1982, **108**, 41
11 Mitchell, G. R. and Windle, A. H. *Polymer* 1983, **24**, 1513
12 Mitchell, G. R. and Windle, A. H., 'Developments in Crystalline Polymers', (Ed. D. C. Bassett), Elsevier Applied Science, London, Vol. II, 1988, 115
13 Bower, D. I., Jarvis, D. A., Lewis, E. L. V. and Ward, I. M. *J. Polym. Sci., Polym. Phys. Edn.* 1986, **24**, 1481
14 Brody, H. and Ward, I. M. *Polym. Eng. Sci.* 1971, **11**, 139
15 Hull, D., 'An Introduction to Composite Materials', Cambridge University Press, Cambridge, 1981, Ch. 6